Shallow flows over a permeable medium: the hydrodynamics of submerged aquatic canopies

Citation: M. Ghisalberti and H. Nepf, "Shallow Flows Over a Permeable Medium: The Hydrodynamics of Submerged Aquatic Canopies," Transport in Porous Media. 78(2), 309-326 (2009)

As Published: http://dx.doi.org/10.1007/s11242-008-9305-x

Publisher: Springer Netherlands

Persistent URL: http://hdl.handle.net/1721.1/49477

Version: Author's final manuscript: final author's manuscript post peer review, without publisher's formatting or copy editing

Transport in Porous Media manuscript No.
(will be inserted by the editor)

Shallow flows over a permeable medium: the hydrodynamics of submerged aquatic canopies

Marco Ghisalberti · Heidi Nepf

Received: date / Accepted: date

Abstract Aquatic flow over a submerged vegetation canopy is a ubiquitous example of flow adjacent to a permeable medium. Aquatic canopy flows, however, have two important distinguishing features. Firstly, submerged vegetation typically grows in shallow regions. Consequently, the roughness sublayer, the region where the drag length scale of the canopy is dynamically important, can often encompass the entire flow depth. In such shallow flows, vortices generated by the inflectional velocity profile are the dominant mixing mechanism. Vertical transport across the canopy-water interface occurs over a narrow frequency range centered around f_v (the frequency of vortex passage), with the vortices responsible for more than three-quarters of the interfacial flux. Secondly, submerged canopies are typically flexible, coupling the motion of the fluid and canopy. Importantly, flexible canopies can exhibit a coherent waving (the *monami*) in response to vortex passage. This waving reduces canopy drag, allowing greater in-canopy velocities and turbulent stresses. As a result, the waving of an experimental canopy reduces the canopy residence time by a factor of four. Finally, the length required for the set-up and full development of mixing-layer-type canopy flow is investigated. This distance, which scales upon the drag length scale, can be of the same order as the length of the canopy. In several flows adjacent to permeable media (such as urban canopies and reef systems), patchiness of the medium is common such that the fully-developed condition may not be representative of the flow as a whole.

Keywords canopy flow · roughness sublayer · flexibility · monami · vortices · vertical transport · residence time · flow development

M. Ghisalberti
School of Environmental Systems Engineering, University of Western Australia, Crawley, Western Australia, Australia.
Tel.: +61-8-64883530
Fax: +61-8-64881015
E-mail: marco.ghisalberti@uwa.edu.au

H. Nepf
Department of Civil and Environmental Engineering, Massachusetts Institute of Technology, Cambridge, MA, USA.

1 Introduction

Canopies of submerged aquatic vegetation represent a permeable medium with high porosity (typically $> 90\%$). Relative to other flows adjacent to permeable media, this high porosity allows rapid vertical transport into the canopy as well as large, and often turbulent, in-canopy flows. The biogeochemical processes within a submerged canopy, as well as the impact of the canopy on the surrounding environment, are regulated, at least in part, by the exchanges of momentum and mass between the canopy and surrounding open water. For example, larval settlement on seagrass depends on the rate at which larvae are delivered into the canopy (Eckman (1987); Grizzle *et al.* (1996)). Also, turbulent mass exchange across the canopy-water interface can regulate the supply of nutrients needed for growth. Bartleson *et al.* (2005) used a numerical model to examine how the rate of water renewal impacted the ecosystem balance within a seagrass meadow. The epiphyte biomass increased with rate of renewal, but the seagrass grew best when exchange rates were low enough to allow nutrient levels to be drawn down within the meadow, which slowed algal growth. The response of submerged macrophytes to changes in nutrient supply was thus shown to be strongly dependent on the rate of fluid exchange between the canopy and surrounding water.

When flow encounters a submerged canopy, the discontinuous canopy drag generates a shear layer across the canopy-water interface. This shear layer is hydrodynamically similar to a plane mixing layer (Raupach *et al.* (1996)). As a result, interfacial transport in canopy flows is dominated by a street of coherent Kelvin-Helmholtz-type vortex structures (Figure 1, see also Gao *et al.* (1989); Ghisalberti and Nepf (2006)). The vortices cause vertical transport to be highly periodic but also, due to their finite lateral extent, spatially non-uniform (Ghisalberti and Nepf (2005)). The frequency of vortex passage (f_v) agrees well with that predicted by linear stability analysis (Ghisalberti and Nepf (2002); White and Nepf (2007)) and is dependent upon the mean flow speed and shear layer thickness.

Particularly in dense canopies, the vortices often do not penetrate completely to the bed. This separates the canopy vertically into two zones (Nepf and Vivoni (2000)). The upper zone (termed the "exchange zone") is flushed rapidly by the vortices and is driven by both the turbulent stress and the hydraulic gradient. The lower zone (termed the "wake zone") is governed by a simple balance of drag and hydraulic gradient, much like classical porous medium flow. The extent of vortex penetration into a submerged canopy (δ_e) is inversely proportional to the drag length scale of the canopy, ($(C_D a)^{-1}$, where C_D is the canopy drag coefficient and a is the frontal area per unit volume). Specifically,

$$\delta_e \approx 0.25\,(C_D a)^{-1} \tag{1}$$

(Nepf *et al.* (2007)). In the absence of vortex-driven transport, mixing in the wake zone is much lower than that in the exchange zone (Nepf and Vivoni (2000)). Canopy residence time is therefore highly dependent upon the fraction of the canopy that is flushed by the vortices. Consequently, $C_D a h$, the scale ratio of canopy height h to exchange zone depth, is a key dimensionless parameter in the description of transport in canopy flows (Nepf *et al.* (2007)).

Drag length scales of real submerged canopies are highly variable. Under the assumption that C_D is $\mathcal{O}(1)$, the drag length scale of marine and freshwater grass canopies typically ranges between $\mathcal{O}(1)$ and $\mathcal{O}(100)$ cm (see, for example, Wu *et al.* (1999); Luhar *et al.* (2008)). For experimental canopies with typical drag length scales

($(C_Da)^{-1} = 16 - 50$ cm), roughly one-third to one-quarter of the mixing layer exists within the canopy (Ghisalberti and Nepf (2004)). Therefore, using Equation (1), $(C_Da)^{-1}$ is an approximate measure of the vortex size.

While the importance of coherent turbulent structures is a characteristic of flows near highly permeable media, flows over submerged aquatic canopies have two important distinguishing features. Firstly, the depth of flow above the canopy ($H - h$, where H is the total flow depth) can be of the same order as the drag length scale. Such shallow flows warrant further attention, as our current understanding of flows over permeable media comes primarily from the study of effectively unbounded flows that are very deep (terrestrial canopies and urban canopies) or over very dense media (packed beds). In §3 of this paper, we contrast vertical transport in shallow canopy flows against that in deep, rough-walled flows.

The second unique feature of aquatic canopy flows arises from the flexibility of the porous medium. Presumably to reduce their drag, submerged canopies tend to be sufficiently flexible that the canopy height is a strong function of flow velocity (see, e.g., Vogel (1984); Denny *et al.* (1998); Stephan and Gutknecht (2002)). While the mean deflection of submerged vegetation in a current can be easily accommodated in numerical models, very little is known about the hydrodynamic impact of a pronounced and coherent waving, the *monami*. This waving is in response to vortex passage, and occurs at the same frequency (Ghisalberti and Nepf (2002)). The *monami* is observed as pockets of plant deflection moving downstream; each pocket corresponds to the strong sweep (a downward and downstream velocity perturbation) at the front of the coherent vortices (Ghisalberti and Nepf (2006)). This unsteadiness of the medium geometry can have a considerable impact on the canopy-scale hydrodynamics. However, most experimental studies to date have employed rigid model vegetation. In §4, we investigate the impact of the *monami* on the salient hydrodynamic and transport properties of a canopy flow.

When flow encounters a submerged canopy, a finite length (L_T) is required for the transition from boundary-layer flow upstream of the canopy to mixing-layer-type flow in the vegetated region. This transition region is characterised by the development of a shear layer across the top of the canopy due to the drag-induced deceleration of fluid within the canopy. Through the growth of the Kelvin-Helmholtz vortices, the thickness of the shear layer grows downstream, reaching its equilibrium size a distance L_T from the front of the canopy (Figure 1(b)). This transition occurs over $\mathcal{O}$(m) in the laboratory (Ghisalberti and Nepf (2002)). Beyond L_T, the velocity profile and vertical transport do not vary with distance from the front of the canopy. Vertical transport in the transition region is considerably different to that in the fully-developed flow. Due to the deceleration of in-canopy fluid during the transition, there is a strong upward advective flux but vortex-driven mixing is expected to be diminished due to the reduced vortex size. The final objective of this work (§5) is to describe the length scale of this transition. Most experiments on canopy flows focus on the region of fully-developed flow. While the equilibrium condition is a good representation of the canopy flow if $L_T \ll L$ (where L is the canopy length), this is not necessarily always the case. In order to describe the hydrodynamic impact of a submerged canopy, it is therefore essential that we have the capacity to predict the scale of L_T.

It is important to note that this analysis pertains only to 'dense' canopies, where canopy drag dominates bed drag and an inflection point is generated in the mean velocity profile. This is the case when $C_Dah \gtrsim 0.1$ (Nepf *et al.* (2007)). Furthermore, this analysis is not applicable to extremely shallow flows, where the free surface restricts

vortex growth. In this approach to the limit of emergent vegetation, wake turbulence begins to dominate shear-layer-scale turbulence within the canopy and δ_e drops below the value given in Equation (1) (Nepf and Vivoni (2000)). In the experimental canopy of Nepf and Vivoni (2000), this was found to be the case when the depth of flow above the canopy ($H - h$) was less than the plant height (h).

2 Experimental conditions

To address the issues discussed in §1, we use previously-conducted canopy flow experiments (Table 1). The run names used here are consistent with Ghisalberti and Nepf (2006), which contains more detail about the model canopies and all runs except FT1, FT2 and R23 (unpublished). All experiments were conducted with a model canopy placed in a unidirectional current in a level flume. The two flumes employed here had cross-sections of 60(W) $\times$ 40(H) cm^2 and 38 $\times$ 58 cm^2. The flow rate ranged between 4700 and 14800 cm^3/s. These experiments were performed with both rigid and flexible model canopies. In naming the experiments, 'R' denotes a rigid canopy, 'F' a flexible canopy and 'T' an experiment to investigate the transitional region. The rigid canopies were composed of wooden dowels. The flexible canopy for experiments F2, F6 and FT2 is shown in Figure 2. It is made from a buoyant plastic and is modelled on *Zostera marina*, a common seagrass (see Ghisalberti and Nepf (2006) for more detail). This flexible model clearly exhibits the *monami*; the depression in the height of the white plants can be seen in Figure 2(b). The canopy for Run FT1 was a dynamically similar model, made from a thinner film of the same plastic (Ghisalberti and Nepf (2002)). In all cases, the length of the model canopy was greater than L_T, allowing the measurement of fully-developed canopy flow.

In each experiment, vertical profiles of ten-minute, 25 Hz velocity records were obtained by acoustic Doppler velocimeters. Points in each profile were separated vertically by $0.5 - 1$ cm. To capture the horizontal variability in canopy flows, profiles were taken at three or four locations separated laterally by tens of centimetres. Experiments FT1 and FT2, where one vertical profile was taken at several streamwise locations, are exceptions. These experiments are used to determine the scale of L_T. With the exception of these runs, the data presented in this paper are temporally-averaged, then horizontally-averaged, statistics. The principal flow direction is x, with z denoting the vertical direction. At each measurement location, velocities in both directions (u and w) are decomposed into long-term temporal averages (U and W) and deviations from these averages (u' and w'). The horizontal average of the relevant statistic is then taken.

In Table 1, the friction velocity is defined as the square root of the maximum in the horizontally-averaged Reynolds stress profile. That is,

$$u_* = \sqrt{\left(-\overline{u'w'}\right)_{max}}, \tag{2}$$

where the overbar indicates a temporal average. The maximum stress occurs at the top of the canopy in these flows. A range of heights is given for the canopies of Runs F2 and F6. In Run F2, where the canopy is flexible but not waving, the range represents the variable extension of the buoyant blades that made up each plant. In Run F6, where waving is observed, the range represents the oscillation of an average plant during the *monami*. In the other flexible canopies (Runs FT1 and FT2), the value of h is a

canopy average measured beyond the transitional zone. The mean interfacial velocity is denoted as U_h; for those runs with a range of heights, U_h is the velocity at the maximum value of h. Finally, the drag length scale of the canopies was evaluated from a momentum balance within the exchange zone, as described in Ghisalberti and Nepf (2006).

3 Vertical transport in canopy flows

The inner layer of flows over rough boundaries is typically considered to consist of three regions: the canopy sublayer (CSL, $0 < z < h$), the roughness sublayer (RSL, $h \lesssim z \lesssim 2-5h$) and the inertial sublayer (ISL, $5h \lesssim z \lesssim 0.2\delta$) (see, e.g., Raupach *et al.* (1991); Cheng and Castro (2002); Britter and Hanna (2003)). Immediately above the canopy, flow in the RSL is characterised by strong three-dimensionality, coherent turbulent structures and the influence of length scales associated with the roughness. In the ISL, the boundary layer has adapted to the integrated effect of the underlying roughness Britter and Hanna (2003). In this region, velocity varies with the logarithm of height and the relevant length scale is height above the canopy (or, more precisely, the height above the zero-plane displacement, d). Relative to the scaling of vertical mixing in the ISL (i.e. $D_z = \kappa u_*(z-d)$), vertical mixing is enhanced in the RSL (Raupach *et al.* (1996)).

A central theme of this paper is that aquatic flows over submerged canopies are generally sufficiently shallow so as to be dominated by the RSL. That is, the effect of the free surface is often to restrict the development of a logarithmic layer and cause the flow to be dominated by the length scales and relatively coherent turbulence associated with the RSL. Due to light requirements, the depth of submerged canopy flows is restricted. Duarte (1991) found that a majority of seagrass species colonise to a depth of 5 m or less. The same holds true for freshwater angiosperms (Chambers and Kalff (1985)). So, despite the height of submerged canopies being highly variable, it is not uncommon for H/h to be less than 5 in canopy flows. In such cases, the RSL will represent most or all of the flow depth and the hydrodynamics will be governed by the drag scale $(C_D a)^{-1}$, rather than by a combination of the drag scale and the flow depth. In the following sections, we discuss fundamental differences between canopy flows and unvegetated open-channel flows, where the RSL typically represents a tiny fraction of the overall flow depth. Firstly, differences in the structure of vertical transport in canopy flow and the ISL are discussed. Secondly, flow in two open channels are contrasted: one with a submerged canopy and one without.

3.1 Impact of a submerged canopy on open-channel flow

The impact of a submerged canopy on vertical transport in open-channel flow is demonstrated in Figure 3. In this figure, vertical profiles of four key hydrodynamic parameters in rough turbulent flow in an unvegetated channel are compared to those in flow over a submerged canopy. The four parameters are: (i) the mean velocity (U), (ii) a characteristic vertical turbulent velocity (w_{rms}), (iii) a characteristic vertical turbulent length scale (the mixing length l_z, defined by $\overline{u'w'} = -l_z^2(\partial U/\partial z)\,|\partial U/\partial z|$) and (iv) the rate of vertical scalar mixing (D_z). As is customary in open-channel flow, each parameter is normalised by H and/or u_{*H}, where $u_{*H}^2 = gHS = u_*^2(H/(H-h))$. Here, S is

the surface slope. In effect, we are comparing two channels (one vegetated and one unvegetated) with the same flow depth and surface slope. The canopy flow characteristics are taken from Run R7, which contains a canopy of moderate density (4% by volume) and submergence ($h/H = 0.3$). With the exception of the velocity profile, the curves for flow in the unvegetated channel are taken from smooth bed data presented in Nezu and Rodi (1986) and Nezu and Nakagawa (1993). Examination of data in rough channels (Fischer *et al.* (1979); Nezu and Nakagawa (1993); Kironoto and Graf (1994)) reveals that, for the qualitative comparison here, typical channel roughnesses do not have a significant impact on these profiles. The velocity profile is computed assuming an equivalent roughness (k_s) of $H/100$. Expressions for the four profiles in an unvegetated flow are given in the Appendix.

The primary hydrodynamic impact of the canopy is the exertion of drag, which significantly reduces the mean channel velocity (Figure 3(a)). For this canopy, with dimensionless density $C_D ah = 0.7$, the mean flow is less than one-third of that over the rough bed. Naturally, this flow reduction is most pronounced near the bed, in the region of drag exertion. The profiles of the vertical turbulent velocity (w_{rms}, Figure 3(b)) are similar in the upper regions of the two flows. Given the significantly lower mean velocity, this similarity implies much higher turbulence intensities in canopy flows. Within the canopy ($z/H < 0.3$), there is a rapid attenuation of vertical turbulent fluctuations. The reduced velocities and turbulence are possibly one reason why canopies of submerged macrophytes typically support a greater abundance and species richness of aquatic fauna than unvegetated areas (Lewis (1984)). The vertical mixing length (l_z, Figure 3(c)) exhibits much less variability in the canopy flow than it does in the unvegetated channel. In the bare channel, where there is a range of eddy scales, the dominant turbulent length scale depends primarily on distance from the boundaries. In canopy flow, however, there is a predominance of a single scale (i.e. the vortex scale). Consequently, the vertical mixing length scales upon the vortex scale (Ghisalberti and Nepf (2004)), which is dictated by canopy characteristics and is of the order of the drag length scale $(C_D a)^{-1}$. At $z \approx h$, the characteristic length scale in the canopy flow is lower than that in the unvegetated channel and the strength of the turbulence is comparable. However, the rate of vertical scalar mixing is significantly *higher* in the canopy flow. This results from greatly different rates of mixing of mass and momentum in canopy flows. In open channels, the turbulent Schmidt number ($\mathrm{Sc}_t = \nu_{tz}/D_z$, where ν_{tz} is the vertical eddy viscosity) is approximately unity (Fischer *et al.* (1979)), indicating equal rates of transport. In canopy flows, mass is mixed much more rapidly than momentum, as in a mixing layer (Raupach *et al.* (1996)). Experimentally, Ghisalberti and Nepf (2005) found that the turbulent Schmidt number in a shallow canopy flow has a mean value of approximately 0.5 and reaches a minimum value of 0.3 at the top of the canopy. That is, mass is mixed across the canopy-water interface three times more rapidly than is momentum. This elevates the rate of vertical scalar mixing into and out of the canopy above that at the same point in the unvegetated channel.

It is important to note that the depth-invariant mixing length is only observed in shallow canopy flows. This is demonstrated in Figure 4, which compares profiles of the vertical mixing length in comparatively shallow (Run R7, $H/h = 3.4$) and deep (Run R23, $H/h = 13.6$) flows. In this figure, the mixing length and height above the canopy have been normalised by the drag length scale. In contrast to the shallow flow, the mixing length in the shear layer of the deep flow increases with height above the canopy. Importantly, the rate of change ($dl_z/dz \approx 0.13$) is much less than that in the ISL ($dl_z/dz = \kappa = 0.41$). So, while deep canopy flows deviate somewhat from the

dominance of a single length scale, they remain dynamically distinct from logarithmic layers.

It stands to reason that if $(C_D a)^{-1}$ describes the vortex scale, then description of the depth of a canopy flow should be based not on the simple ratio H/h but on the ratio of the depth of the overflow to the vortex scale (i.e. $C_D a(H-h)$). In Figure 4, the shallow flow has a depth ratio of 1.6 and the deep flow a ratio of 7.3. Similarly, in other rough-walled flows where the bed does not impede vortex growth (i.e. $C_D ah \gtrsim 0.3$), it would seem that extension of the RSL above the roughness should scale upon $(C_D a)^{-1}$, not h. Indeed, Raupach *et al.* (1991) note that the vertical extent of the RSL above the canopy (as a multiple of h) is highly variable and lower for dense canopies. This suggests that it is in fact the drag length scale of the canopy that dictates the vertical extent of the RSL.

3.2 Periodicity of momentum transport

The cospectrum of u and w (Co_{uw}) reveals that the coherent vortices are responsible for the majority of interfacial transport in canopy flows. In Figure 5, the normalised cospectrum at the top of the canopy in Run R7 is shown. The presented cospectrum is the average of six individual realisations from two measurement points (immediately above and below the canopy top) in three vertical profiles. The cospectrum is relatively narrow-banded about the frequency of vortex passage (f_v), shown from individual spectra of u and w to be approximately 0.07 Hz. The cospectrum exhibits clear peaks at both f_v and $2f_v$. As shown in Ghisalberti and Nepf (2006), each vortex consists of two downward transport events, a strong sweep ($u' > 0$, $w' < 0$) followed by a weaker ejection ($u' < 0$, $w' > 0$). The peak at twice f_v arises from the two stress events per vortex; the differential strength of the two events generates the peak at f_v.

Integration of the cospectrum is used to determine the fraction of vertical interfacial transport generated by the coherent vortices. The vortices are deemed to be responsible for all energy in the cospectrum below a (nominal) frequency of $3f_v$. This limit allows the full incorporation of the higher frequency peak into the vortex contribution. As the flow is sufficiently shallow to prevent the development of an ISL, the vortex is the turbulent structure in the flow with the lowest frequency. All energy above $3f_v$ is deemed to be generated by incoherent, smaller-scale turbulence. The coherent vortices generate 80% of the interfacial momentum transport in Run R7 ($C_D ah = 0.7, \mathrm{Re} = u_*(C_D a)^{-1}/\nu = 3 \times 10^3$). This contribution appears to be invariant in the shallow canopy flows studied here (i.e. those for which $C_D a(H-h) \sim \mathcal{O}(1)$). For example, the fraction is insensitive to canopy density, with the vortices contributing 78% of transport in Run R1 ($C_D ah = 0.3$). Likewise, flows with vastly different Reynolds numbers (Run R9, $\mathrm{Re} = 8 \times 10^2$, 75%) and even canopy flexibility (Run F6, waving canopy, 75%) have similar contributions. However, in the deep flow (Run R23, $C_D a(H-h) = 7.3$), the vortex contribution is less than 60%. Using this description of vortex influence based on the uw-cospectrum, the coherent vortices are the dominant mechanism for vertical transport into and out of submerged canopies in shallow flows. Accordingly, our characterisation of these flows is based largely upon the length and velocity scales of the vortices. It remains to be seen if the vortices are responsible for a similar fraction of scalar transport. While the deviation of the turbulent Schmidt number from unity (§3.1) suggests fundamental differences in mass and momentum transport in canopy

flow, time series of in-canopy concentration show clear peaks at the vortex frequency (Ghisalberti and Nepf (2005)).

In Figure 5, the cospectrum of canopy flow is compared to that in a logarithmic ISL. The inertial sublayer cospectrum, evaluated for at a point a distance h from a solid boundary with a mean velocity equal to U_h in Run R7, is taken from Kaimal and Finnigan (1994). The comparison demonstrates that the dominance of vertical mixing by low-frequency processes is not unique to canopy flows. Indeed, there is a greater contribution from low frequencies in the ISL, with 88% of the momentum flux at frequencies below the nominal cutoff ($3f_v \approx 0.2$ Hz). What is characteristic of canopy flows is the narrow-bandedness of the transport. Significant vertical transport occurs over only two decades of frequency, as opposed to nearly three decades in the ISL.

4 Impact of canopy flexibility

4.1 Hydrodynamics

Most experimental investigations of canopy flows employ a rigid model canopy. The steady geometry of an inflexible canopy permits an unequivocal definition of the canopy-water interface, an easily-calculated frontal density and a reasonable estimate of the drag coefficient. However, these models are not fully representative of real submerged canopies. A recent experimental study by Ghisalberti and Nepf (2006) has shown that canopy waving reduces drag and causes a reduction in interfacial mixing. However, it is difficult to explicitly determine the hydrodynamic impact of the *monami* from experimental data alone. For a given model canopy the surface slope and flow speed required to trigger the *monami* are much greater, and the plant height smaller, than those in the absence of waving. For example, in going from Run F2 (no waving) to Run F6 (waving), the surface slope increases by a factor of 4.6 and the average canopy height decreases by 35%.

In this section, we contrast the hydrodynamics of two submerged canopies (one waving and one inflexible) in open channels with the same slope and flow depth. As described above, it is difficult to make this comparison from experimental data alone. So, we compare the experimental data from a waving canopy (Run F6) to the numerical model prediction for the flow if the canopy were inflexible. To allow this comparison, it is vital that we can faithfully model the key characteristics (e.g. profiles of velocity and stress) of flow over an inflexible model canopy. Here, the model of Defina and Bixio (2005)[1] (DBM) is employed. This two-layer model assumes a logarithmic velocity profile above the canopy. Although the flow immediately above the canopy does not satisfy the conditions of an ISL, a logarithmic form can be used to adequately describe the velocity profile (e.g. Shi *et al.* (1995); Stephan and Gutknecht (2002)). Within the canopy, the 1-D momentum equation is solved assuming an eddy viscosity that scales on the product of the local velocity (U) and the plant height (h). While our experiments (Ghisalberti and Nepf (2004)) show that the more relevant scales for the eddy viscosity are u_* and $(C_D a)^{-1}$, the fully empirical closure of the DBM performs well across a range of canopy densities and heights (Meijer and van Velzen (1999)). The velocity and velocity gradient are matched at the canopy interface, which dictates the values

[1] In Equation (21) of this paper there is a typographical error, confirmed by the authors (*pers. comm.*). In the denominator of the coefficient, h_p should in fact be h_p^2.

of the zero-plane displacement and roughness height in the logarithmic profile. Model validation was achieved by comparing the model profiles of velocity and stress for the non-waving canopy of Run F2 to those measured experimentally. As input, the model requires the surface slope ($S = 1.6 \times 10^{-5}$ in this case), the flow depth (46.7 cm), the value of $C_D a$ (0.060 cm^{-1}) and the canopy height. As discussed in §2, the canopy of Run F2 has a range of heights due to the variable extension of the buoyant plant blades. The lowest plant height (19.5 cm), the point of maximum turbulent stress, was chosen as the height input for this model. As shown in Figure 6(a), the velocity profile of Run F2 is predicted particularly well, both within and above the canopy. Figure 6(b) shows that there is a slight discrepancy between the two stress profiles within the canopy. The important factor in this comparison, though, is the depth of penetration of turbulent stress. This penetration of vortex-driven flushing is a major control of canopy residence time. The prediction of penetration depth agrees very well with the experimental data; both profiles reach negligible stress values at $z \approx 10$ cm. So, in discussing the impact of the *monami* on canopy hydrodynamics, we are confident that the DBM will provide realistic estimates of the velocity profile and the depth of the exchange zone in nonwaving canopies.

Given this confidence in the DBM, we can clearly shed light upon the hydrodynamic impact of canopy waving. Two open channels with submerged canopies and the conditions of Run F6 ($H = 46.7$ cm and $S = 7.4 \times 10^{-5}$) are compared. One submerged canopy is waving, the other is inflexible. Flow characteristics for the channel with the inflexible canopy are generated by the DBM; those for the channel with the flexible canopy are taken from experimental measurements. Although the flow depth in a real channel of constant slope would vary with the bottom roughness, the relationship between flow depth and slope (a Manning's-n-type formulation) remains virtually unknown for flexible, submerged canopies. So, for simplicity, the flow depths in the two channels are the same. Flexibility aside, the two canopies are identical ($a = 0.052$ cm^{-1}, $h_{max} = 15.5$ cm). In the case of the waving canopy, the change in canopy height over the *monami* cycle was 4.4 cm (nearly 30% of h_{max}). As discussed, this waving causes a decrease in canopy drag. For the waving canopy, the mean value of $C_D a$ in the exchange zone is 0.034 cm^{-1} (Ghisalberti and Nepf (2006)). The measured value of $C_D a$ for the non-waving canopy of Run F2 was 0.060 cm^{-1}; the inflexible canopy in this comparison is assigned the same value.

Clearly, the reduced drag of the waving canopy permits a higher mean velocity that the inflexible canopy (Figure 6(c)). The average in-canopy velocity (i.e. that in the region $0 < z < h_{max}$) increases by 65% due to the 40% reduction in canopy drag due to waving. This velocity difference is most pronounced at the minimum plant height in the *monami* cycle ($z \approx 11$ cm), where the velocity in the waving canopy (5.4 cm/s) is double that in its inflexible counterpart (2.7 cm/s). The *monami* also drastically increases the depth of the exchange zone (Figure 6(d)). Defined as the depth over which $-\overline{u'w'}$ decays to 10% of its maximum, interfacial value, δ_e increases from 5.9 cm to 11.7 cm with canopy waving. It is important to note that this increase is *more* than the amplitude of the *monami*; dynamically, waving is more than a simple downshift of the canopy-water interface. The *monami* causes the canopy to behave as if sparser, allowing greater velocities and vortex penetration.

4.2 Canopy residence time

Due to the increased stress penetration into the canopy, it is expected that waving will dramatically reduce the canopy residence time. To quantify this reduction, the vertical transport model of Nepf *et al.* (2007) (VTM) is employed. This two-box model separates the canopy into the exchange zone and the wake zone; the boundary between the two boxes is at $z = h - \delta_e$. The exchange velocity between the wake zone and the exchange zone is based on the diffusivity in an emergent canopy, which scales upon the flow speed (U_1) and the plant diameter. The exchange velocity (k_e) between the exchange zone and the water overlying the canopy is $0.19u_*(C_D ah)^{0.13}$. It is important to note here that the interfacial stress (and thus u_* and k_e) is higher for nonwaving canopies. This is indicative of the diminished interfacial transport in waving canopies, the unsteady geometry presumably reducing vortex coherence (Ghisalberti and Nepf (2006)). Using the methodology of Nepf *et al.* (2007), the canopy is originally given a uniform scalar concentration (C_o) with zero concentration above the canopy at all times. The decrease in the depth-averaged concentration in the canopy (C) is then monitored over time. Implicit in this analysis is the assumption that the canopy is of sufficient horizontal scale that flushing of the canopy is dominated by vertical mixing.

Firstly, it is important to ensure that the DBM-predicted values of u_*, δ_e and U_1 (the wake zone velocity) give a description of residence time in nonwaving canopies that is consistent with that from the experimental data. The VTM was run for the conditions of Run F2 with both experimental data (see Ghisalberti and Nepf (2006)) as well as with the values predicted by the DBM. The comparison of decay curves of C/C_o for the model data and experimental data is displayed in Figure 7(a). The agreement is very good both in the short term (when the interfacial flux is dictated by flushing of the exchange zone) and the long term (when the flux is controlled by diffusion from the wake zone). With this confidence in the ability of the DBM to provide reasonable input values to the vertical transport model, we use the VTM to investigate the impact of the *monami* on the canopy residence time. Figure 7(b) compares the decay of in-canopy concentration for a waving and nonwaving canopy in a channel with the conditions of Run F6 (refer to the previous section). For averaging purposes, the height of both canopies is taken as 15.5 cm. Despite the diminished interfacial mixing, it is clear that the waving canopy is flushed much more rapidly. This is due primarily to the fact that the *monami* permits a much deeper exchange zone than the nonwaving canopy. Using the time at which C drops to 10% of its initial value as a nominal description of residence time, the residence time in the nonwaving canopy (1520 s) is more than four times that in the waving canopy (370 s).

To our knowledge, there have been no direct measurements of vertical diffusivity in the wake zone of a submerged canopy. The transport model employed here requires as input this wake zone diffusivity. It is assumed to be the same as that measured in emergent canopies, which are similarly governed by a balance of hydraulic gradient and canopy drag. In the same way that oscillatory flows increase solute fluxes from sediment beds (Webster and Taylor (1992)), it is conceivable that mixing in the wake zone may be elevated due to the oscillating pressure generated by the vortex street. Although the diffusivity profiles shown in Ghisalberti and Nepf (2005) (and Figure 3(d)) do not extend down to the wake zone, they show a rapidly diminishing diffusivity as the wake zone is approached. So, while there is no direct evidence to inform us on exactly how low the wake zone diffusivity is, it is undoubtedly lower than that in the exchange zone. Accordingly, it is clear that the *monami* will reduce the canopy residence time,

provided that there is a wake zone in the nonwaving canopy (i.e. that $C_D a h \gtrsim 0.3$). The *monami* reduces residence time by allowing the erosion, or elimination, of the wake zone and its comparatively slow mixing.

5 Transition at the front of the canopy

In this section, we examine the length scale of transition at the front of a submerged canopy. By balancing canopy drag with streamwise advection, Belcher *et al.* (2003) derived a characteristic length scale for fluid deceleration (x_0) at the front of a canopy. Coceal and Belcher (2004)[2] performed numerical experiments to determine the scaling coefficient and found that

$$x_0 \approx 6(C_D a)^{-1} \ln\left(C_D a h \left[\frac{U_h}{2u_*}\right]\right) \tag{3}$$

However, it is not just fluid deceleration that governs the transition to equilibrium in canopy flows. A second process occurs, namely the growth of the vortex street and the mixing-layer-type region that it defines. Only once layer growth ceases can the flow be considered fully-developed.

We view this shear layer growth as the vertical turbulent diffusion of vorticity generated at the top of the canopy. Denoting the final thickness of the vortices and mixing-layer-type flow as t_{ml}, the diffusive time scale is given by

$$t_{diff} = \frac{t_{ml}^2}{D_z} \approx \frac{(C_1 \delta_e)^2}{D_z} \tag{4}$$

where D_z is a characteristic vertical turbulent diffusivity. As discussed in §1, C_1, the coefficient that links the final vortex penetration (δ_e) to the total vortex size (t_{ml}), has a value of $3-4$ in canopies of typical density. To first order, the assumption of C_1 as a constant is reasonable. The vertical diffusivity in the fully-developed region scales on the total shear across the canopy (ΔU) and the shear layer thickness (t_{ml}) (Ghisalberti and Nepf (2005)). Ignoring a very slight dependence upon canopy density, ΔU scales upon u_* (Nepf *et al.* (2007)). Although mixing in the transitional region is likely lower than that in the fully-developed flow, we would expect the same scaling to apply. Therefore, a reasonable scaling relationship for the vertical diffusivity in Equation (4) is $D_z \sim u_* \delta_e$. So, if shear layer growth is deemed to be the rate-limiting step in the transition to fully-developed flow,

$$L_T = U_h \times t_{diff} \sim \frac{\delta_e U_h}{u_*}. \tag{5}$$

Here, the characteristic mean advective velocity is U_h, the velocity at the top of the canopy. Given the dependence of δ_e on the drag length scale $(C_D a)^{-1}$ (Equation (1)), the length scale for transition becomes

$$L_T \sim \left(\frac{U_h}{u_*}\right)(C_D a)^{-1}. \tag{6}$$

In defining this relationship, the fully-developed values of U_h and u_* are used.

[2] It is worth noting that the authors use a drag length scale that reduces, in the limit of sparse canopies, to $2(C_D a)^{-1}$ (twice the value of our drag scale).

To determine the scaling coefficient in Equation (6), we use data from Runs FT1 and FT2 (Table 1), where flow properties were measured along the transitional zone of a flexible model canopy. This data is displayed in Figure 8. Two properties that characterise the evolution of the canopy flow are shown. Firstly, the local total shear ($\Delta U(x)$), normalized by the fully-developed advective velocity (U_h), is a measure of the adjustment of the velocity profile to the canopy drag. Secondly, the momentum thickness of the shear layer ($\theta(x)$), normalised by the drag length scale ($(C_D a)^{-1}$), is a measure of shear layer growth through the spreading of vorticity. The distance from the front of the canopy, x, has been normalised according to Equation (6) with fully-developed values of u_* and U_h. It is clear from Figure 8 that the deceleration of in-canopy fluid (and thus the increase of ΔU) occurs more rapidly than the vertical spread of vorticity. For these two runs, the Coceal and Belcher (2004) model predicts deceleration lengths of 0.1 and 0.4 on the normalized x-scale; this is highlighted by the shaded region in the figure. While it can be argued that the shear stops growing not far downstream of that region, the same can not be said of the shear layer thickness. That is, x_0 underestimates the total length of transition in canopy flows. As shown in Figure 8, the length of the transitional zone at the front of the canopy is given by

$$L_T \approx 3 \left(\frac{U_h}{u_*} \right) (C_D a)^{-1} \tag{7}$$

It is important to note that the coefficient in this relationship has been obtained from streamwise transects in flexible, waving canopies. While we expect the same scaling relationship to hold for rigid canopies, the coefficient may differ slightly.

For a sparse canopy, it is possible that L_T represents a significant component (or all of) the canopy length. For river grasses, $(C_D a)^{-1}$ typically ranges between 0.1 and 1 m (see, for example, Wu *et al.* (1999)). While the ratio of U_h to u_* is a function of canopy density, the term $3\,(U_h/u_*)$ is $\mathcal{O}(10)$ in all of the runs detailed in Table 1. Therefore, L_T in a real submerged canopy will be $\mathcal{O}(1 - 10$ m). Indeed, the data of Sukhodolov and Sukhodolova (2006) show a vegetated shear layer continuing to grow $\mathcal{O}(10$ m) into a real river grass canopy. Patchiness of plant canopies, typically on the scale of metres to tens of metres, is common to all aquatic habitats (see, e.g., Duarte and Sand-Jensen (1990); Sand-Jensen and Mebus (1996)). Consequently, a vegetated river flow might not be accurately described by the fully-developed state, but rather by a continual set-up and set-down of mixing-layer-type flow.

6 Conclusions

In this study, experiments with rigid and flexible model vegetation have been used to describe some distinguishing hydrodynamic features of aquatic canopy flows. In shallow flows, where $C_D a(H - h)$ is $\mathcal{O}(1)$, the coherent vortices dominate interfacial transport. Cospectra of u and w are narrow-banded and centered about the frequency of vortex passage. The relevant length scale throughout almost the entire depth of such flows is the drag length scale $(C_D a)^{-1}$, which is an approximate measure of vortex size. In deeper flows, there is a transition away from the predominance of vortex-driven transport and a single turbulent length scale.

Vortex passage drives a coherent, periodic waving of flexible vegetation. In the waving canopy studied (Run F6), the amplitude of the *monami* was nearly 30% of the

maximum plant height. The resultant 40% reduction in canopy drag allowed significant increases in the mean in-canopy velocity and the penetration of turbulent stress. Waving caused a four-fold reduction in canopy residence time due to erosion of the wake zone, whose thickness is the determinant of residence time in tall canopies.

Finally, the transition from boundary-layer flow upstream of the canopy to a mixing-layer-type flow within the canopy was investigated. The growth of the mixing layer, rather than the deceleration of in-canopy fluid, was found to be the rate-limiting process. The length scale of this transition for a waving canopy is approximately $3\,(U_h/u_*)\,(C_D a)^{-1}$.

Acknowledgements This material is partially based on work supported by the National Science Foundation under Grant No. OCE-0751358. Any conclusions or recommendations expressed in this material are those of the author(s) and do not necessarily reflect the views of the National Science Foundation.

Appendix

The curves presented in Figure 3 for open-channel flow are described more fully in Table 2.

References

R.D. Bartleson, W.M. Kemp, and J.C. Stevenson. Use of a simulation model to examine effects of nutrient loading and grazing on *Potamogeton perfoliatus* L. communities in microcosms. *Ecol. Model.*, 185:483–512, 2005.

S.E. Belcher, N. Jerram, and J.C.R. Hunt. Adjustment of a turbulent boundary layer to a canopy of roughness elements. *J. Fluid Mech.*, 488:369–398, 2003.

R.E. Britter and S.R. Hanna. Flow and dispersion in urban areas. *Annu. Rev. Fluid Mech.*, 35:469–496, 2003.

P.A. Chambers and J. Kalff. Depth distribution and biomass of submersed aquatic macrophyte communities in relation to Secchi depth. *Can. J . Fish. Aquat. Sci.*, 42:701–709, 1985.

H. Cheng and I.P. Castro. Near wall flow over urban-like roughness. *Bound.-Layer Meteorol.*, 104:229–259, 2002.

O. Coceal and S.E. Belcher. A canopy model of mean winds through urban areas. *Q. J. R. Meteorol. Soc.*, 130:1349–1372, 2004.

A. Defina and A.C. Bixio. Mean flow and turbulence in vegetated open channel flow. *Water Resour. Res.*, 41, W07006, doi:10.1029/2004WR003475, 2005.

M. Denny, B. Gaylord, B. Helmuth, and T. Daniel. The menace of momentum: Dynamic forces on flexible organisms. *Limnol. Oceanogr.*, 43(5):955–968, 1998.

C.M. Duarte and K. Sand-Jensen. Seagrass colonization: patch formation and patch growth in *Cymodocea nodosa*. *Mar. Ecol. Prog. Ser.*, 65:193–200, 1990.

C.M. Duarte. Seagrass depth limits. *Aquat. Bot.*, 40:363–377, 1991.

J.E. Eckman. The role of hydrodynamics in recruitment, growth, and survival of *Argopecten irradians* (L.) and *Anomia simplex* (D'Orbigny) within eelgrass meadows. *J. Exp. Mar. Biol. Ecol.*, 106(2):165–191, 1987.

http://www.ocean.udel.edu/cms/jgallagher/tigani/kt_index.html. February 27, 2008.

H.B. Fischer, E.J. List, R.C.Y. Koh, J. Imberger, and N.H. Brooks. *Mixing in inland and coastal waters*. Academic Press, San Diego, CA, 1979.

H.B. Fischer. Longitudinal dispersion and turbulent mixing in open-channel flow. *Annu. Rev. Fluid Mech.*, 5:59–78, 1973.

W. Gao, R.H. Shaw, and K.T. Paw U. Observation of organized structure in turbulent flow within and above a forest canopy. *Bound.-Layer Meteorol.*, 47:349–377, 1989.

M. Ghisalberti and H.M. Nepf. Mixing layers and coherent structures in vegetated aquatic flows. *J. Geophys. Res.*, 107(C2):3–1–3–11, 2002.

M. Ghisalberti and H.M. Nepf. The limited growth of vegetated shear layers. *Water. Resour. Res.*, 40, W07502, 2004.

M. Ghisalberti and H. Nepf. Mass transport in vegetated shear flows. *Environ. Fluid Mech.*, 5(6):527–551, 2005.

M. Ghisalberti and H. Nepf. The structure of the shear layer in flows over rigid and flexible canopies. *Environ. Fluid Mech.*, 6:277–301, 2006.

R. Grizzle, F. Short, C. Newell, H. Hoven, and L. Kindblom. Hydrodynamically induced synchronous waving of seagrasses: 'monami' and its possible effects on larval mussel settlement. *J. Exp. Mar. Biol. Ecol.*, 206:165–177, 1996.

J.C. Kaimal and J.J. Finnigan. *Atmospheric Boundary Layer Flows: Their Structure and Measurement*. Oxford University Press, New York, New York, USA, 1994.

B.A. Kironoto and W.H. Graf. Turbulence characteristics in rough uniform open-channel flow. *Proc. Instn Civ. Engrs Wat. Marit. & Energy*, 106:333–344, 1994.

F.G. Lewis. Distribution of macrobenthic crustaceans associated with *Thalassia*, *Halodule* and bare sand substrata. *Mar. Ecol. Prog. Ser.*, 19:101–113, 1984.

M. Luhar, J. Rominger, and H. Nepf. Interaction between flow, transport and vegetation spatial structure. in press, *Environ. Fluid Mech.*, 2008.

D.G. Meijer and E.H. van Velzen. Prototype-scale flume experiments on hydraulic roughness of submerged vegetation. In *Proceedings of XXVIII Congress, International Association for Hydraulic Research*, Graz, Austria, 1999.

H.M. Nepf and E.R. Vivoni. Flow structure in depth-limited, vegetated flow. *J. Geophys. Res.*, 105(C12):28547–28557, 2000.

H. Nepf, M. Ghisalberti, B. White, and E. Murphy. Retention time and dispersion associated with submerged aquatic canopies. *Water Resour. Res.*, 43, W04422, 2007.

I. Nezu and H. Nakagawa. *Turbulence in open-channel flows*. A.A. Balkema, Rotterdam, the Netherlands, 1993.

I. Nezu and W. Rodi. Open-channel flow measurements with a laser doppler anemometer. *J. Hydraul. Eng.-ASCE*, 112(5):335–355, 1986.

M.R. Raupach, R.A. Antonia, and S. Rajagopalan. Rough-wall turbulent boundary layers. *Appl. Mech. Rev.*, 44:1–25, 1991.

M.R. Raupach, J.J. Finnigan, and Y. Brunet. Coherent eddies and turbulence in vegetation canopies: the mixing-layer analogy. *Bound.-Layer Meteorol.*, 78:351–382, 1996.

K. Sand-Jensen and J.R. Mebus. Fine-scale patterns of water velocity within macrophyte patches in streams. *Oikos*, 76(1):169–180, 1996.

Z. Shi, J.S. Pethick, and K. Pye. Flow structure in and above the various heights of a saltmarsh canopy: A laboratory flume study. *J. Coast. Res.*, 11:1204–1209, 1995.

U. Stephan and D. Gutknecht. Hydraulic resistance of submerged flexible vegetation. *J. Hydrol.*, 269:27–43, 2002.

A. Sukhodolov and T. Sukhodolova. Evolution of mixing layers in turbulent flow over submersed vegetation: Field experiments and measurement study. In R.M.L. Ferreira, E.C.T.L. Alves, J.G.A.B. Leal, and A.H. Cardoso, editors, *River Flow 2006: Proceedings of the International Conference on Fluvial Hydraulics*, pages 525–534, 2006.

S. Vogel. Drag and flexibility in sessile organisms. *Am. Zool.*, 24(1):37–44, 1984.

I.T. Webster and J.H. Taylor. Rotational dispersion in porous media due to fluctuating flows. *Water Resour. Res.*, 28(1):109–119, 1992.

B.L. White and H.M. Nepf. Shear instability and coherent structures in shallow flow adjacent to a porous layer. *J. Fluid Mech.*, 593:1–32, 2007.

F.-C. Wu, H.W. Shen, and Y.-J. Chou. Variation of roughness coefficients for unsubmerged and submerged vegetation. *J. Hydraul. Eng.*, 125(9):934–942, 1999.

Table 1 Summary of canopy flow experiments.

Run	$C_D a$ (cm^{-1})	h (cm)	H (cm)	u_* (cm/s)	U_h (cm/s)	Canopy type
R1	0.020	13.9	46.7	0.45	2.5	Rigid
R7	0.049	13.8	46.7	1.6	6.3	Rigid
R9	0.063	13.8	46.7	0.50	2.1	Rigid
R23	0.20	3.0	40.0	0.54	2.4	Rigid
F2	0.060	19.5-21.3	46.7	0.53	3.0	Flexible, not waving
F6	0.034	11.1-15.5	46.7	1.1	7.9	Flexible, waving
FT1	0.043	9.0	41.3	0.79	4.5	Flexible, waving
FT2	0.039	13.3	46.7	1.1	6.4	Flexible, waving

Table 2 Hydrodynamic properties of open-channel flows presented in Figure 3. (NN = Nezu and Nakagawa (1993); NR = Nezu and Rodi (1986))

Parameter	Profile	Source	Notes
U	$\frac{U}{u_*} = \frac{1}{\kappa} \ln\left(\frac{z}{k_s}\right) + 8.5 + \frac{2\Pi}{\kappa} \sin^2\left(\frac{\pi z}{2H}\right)$	NN	Typical values of $k_s/H = 0.01$ and $\Pi = 0.1$ were chosen
w_{rms}	$\frac{w_{rms}}{u_*} = 1.27 \exp(-z/H)$	NN	
l_z	$\frac{l_z}{H} = \frac{\kappa\sqrt{1-(z/H)}}{(H/z) + \pi\Pi \sin(\pi z/H)}$	NR	
D_z	$\frac{D_z}{u_* H} = \frac{\kappa(1-(z/H))}{(H/z) + \pi\Pi \sin(\pi z/H)}$	NN	This expression was derived by assuming that Sc_t is unity for open-channel flow, as seen in Fischer (1973)

(a) The visualisation of a vortex above a rigid canopy through the injection of food dye. These vortices dominate the transport of mass and momentum across the canopy-water interface.

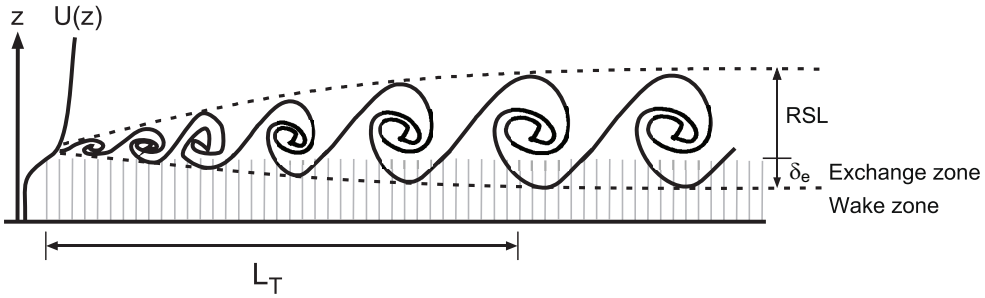

(b) The growth of the vortices along the canopy. At a distance L_T from the front of the canopy, the vortices reach their equilibrium size and the canopy flow is fully-developed. The exchange zone is the region of the canopy that is rapidly flushed by the vortices. The roughness sublayer (RSL), characterised by three-dimensionality and the importance of roughness length scales, extends at the very least to the top of the vortices.

Fig. 1 The street of Kelvin-Helmholtz-type vortices in canopy flows.

(a) (b)

Fig. 2 Photographs of (a) a meadow of *Zostera marina* ("eelgrass", eel (2008)) and (b) the flexible model canopy of Runs F2, F6 and FT2. The model was designed to have the same ratio of buoyancy to flexibility as eelgrass. The model plants are coloured to facilitate visualisation of the *monami*; they are otherwise identical.

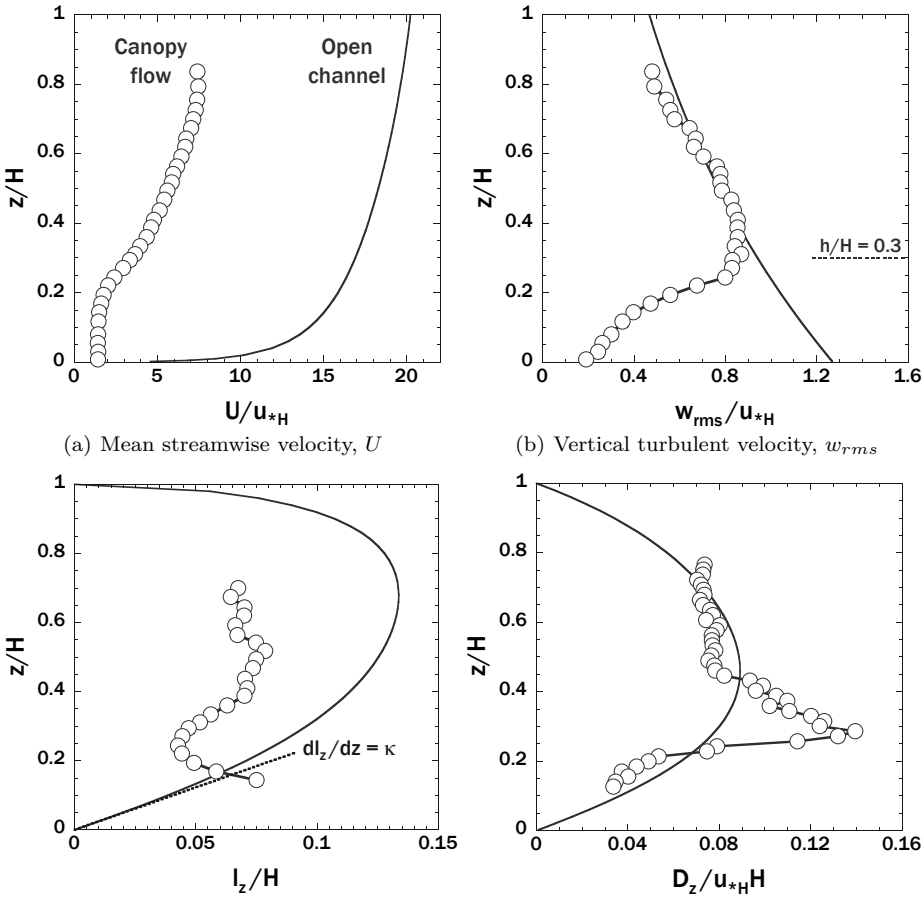

(a) Mean streamwise velocity, U

(b) Vertical turbulent velocity, w_{rms}

(c) Vertical mixing length, l_z

(d) Vertical turbulent diffusivity, D_z

Fig. 3 Comparison of vertical profiles of four hydrodynamic parameters in a canopy flow (Run R7, circles) and an unvegetated open-channel flow (solid line). The canopy takes up 30% of the flow depth.

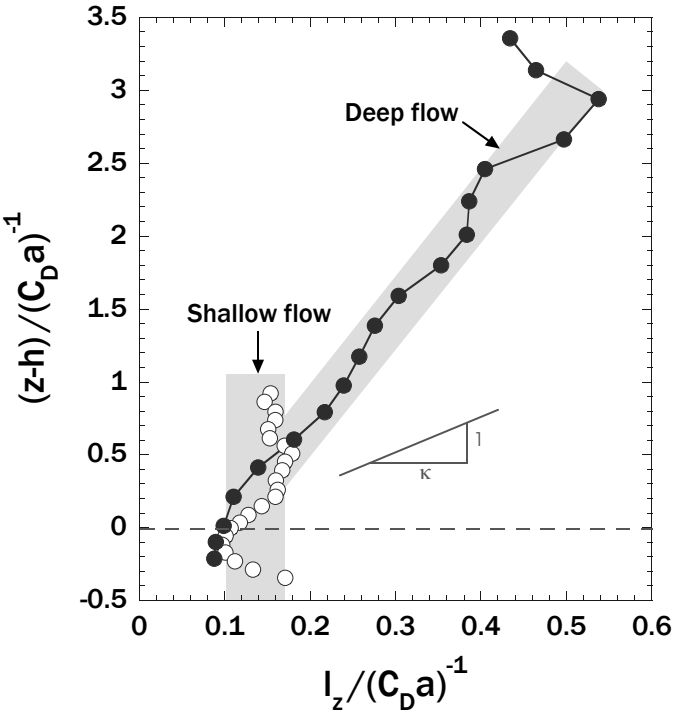

Fig. 4 The vertical profiles of mixing length for a shallow (Run R7, $C_D a(H-h) = 1.6$) and a deep (Run R23, $C_D a(H-h) = 7.3$) canopy flow. The dashed line represents the top of the canopy. The invariant mixing length of the shallow flow is characteristic of canopy flows where the RSL extends to the free surface. Even well above the canopy in the deep flow, ISL behaviour ($dl_z/dz = \kappa = 0.41$) is not observed.

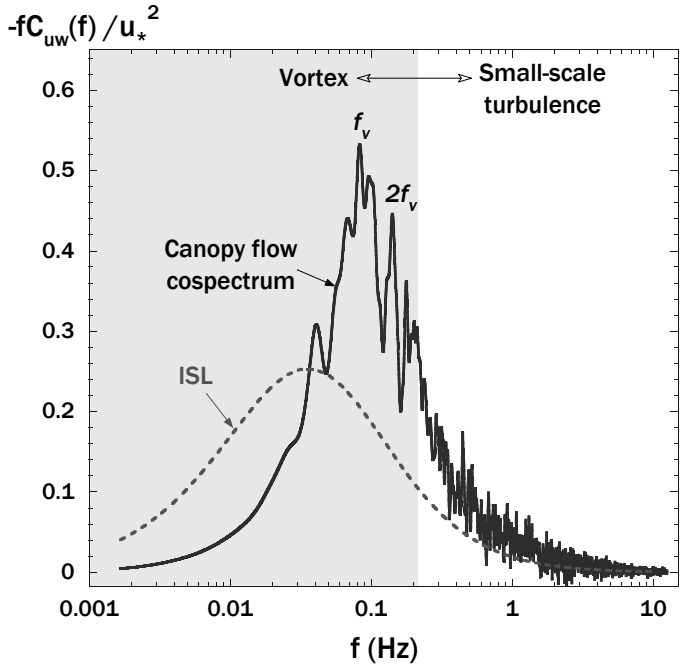

Fig. 5 The normalised cospectrum of u and w at the top of the canopy (Run R7). The narrow-banded cospectrum is centered around peaks at f_v, the frequency of vortex passage, and $2f_v$. Using $3f_v$ as a nominal cutoff for vortex influence, 78% of the area under the cospectrum (and therefore of the interfacial momentum transport) is generated by the vortices. The cospectrum in an inertial sublayer reveals no such dominant frequency in vertical transport.

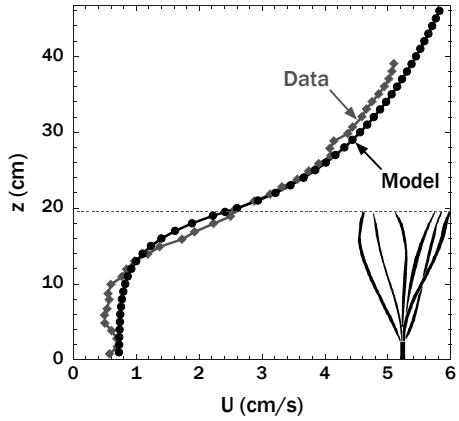

(a) Velocity profile from Run F2 (nonwaving canopy, $h = 19.5$ cm) compared to the DBM prediction.

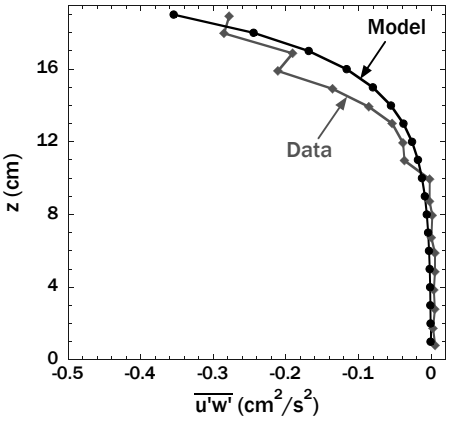

(b) In-canopy stress profile from Run F2 compared to the DBM prediction.

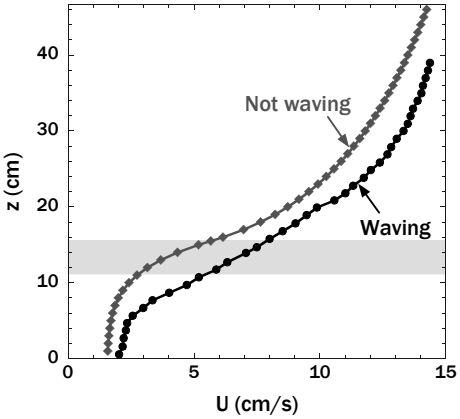

(c) Velocity profile from Run F6 (waving canopy) compared to the DBM prediction if the same canopy were not waving. The shaded region represents the height oscillation through the *monami* cycle.

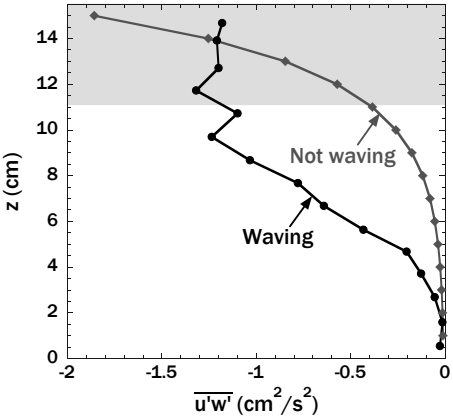

(d) In-canopy stress profile from Run F6 compared to the DBM prediction if the same canopy were not waving.

Fig. 6 The impact of the *monami* on canopy flow hydrodynamics. Firstly, the DBM predicts velocity and stress profiles well in a flow with a nonwaving canopy (a,b). This model is then used to predict the flow behaviour if the canopy of Run F6 were not waving. The *monami* permits much greater (c) in-canopy flow and (d) stress penetration into the canopy.

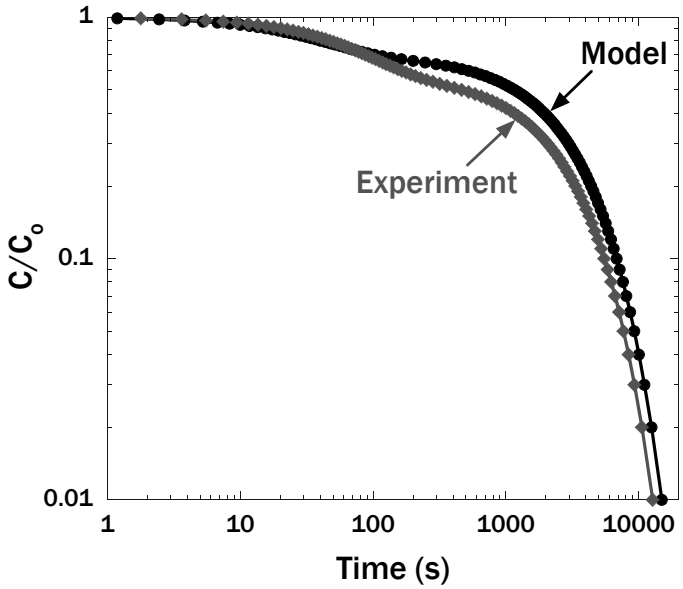

(a) The VTM is applied to the canopy of Run F2 using measured flow parameters as well as those from the hydrodynamic model (DBM). The agreement between the two decay curves is very good, suggesting that the DBM provides values that accurately estimate the residence time of nonwaving canopies.

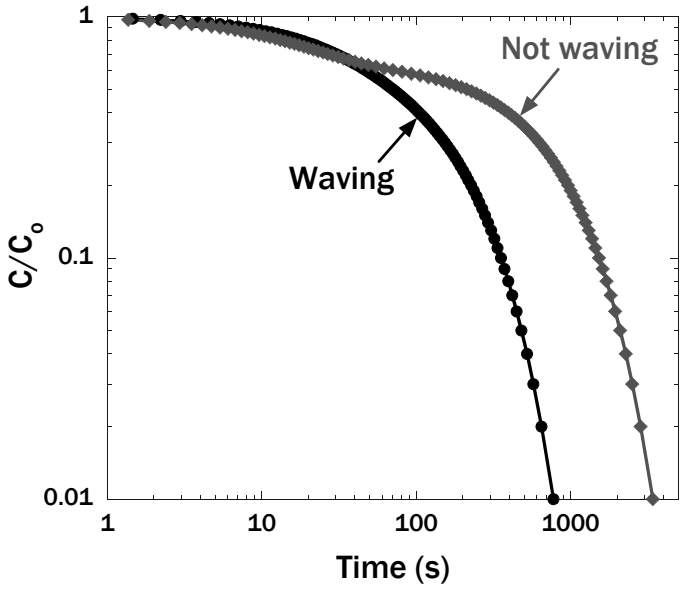

(b) The impact of the *monami* on canopy residence time (Run F6). Nominally defining canopy residence time as the point at which concentration falls to 10% of its initial value, waving decreases residence time by a factor of 4 here.

Fig. 7 The decay of in-canopy concentration C using the two-layer vertical transport model (VTM).

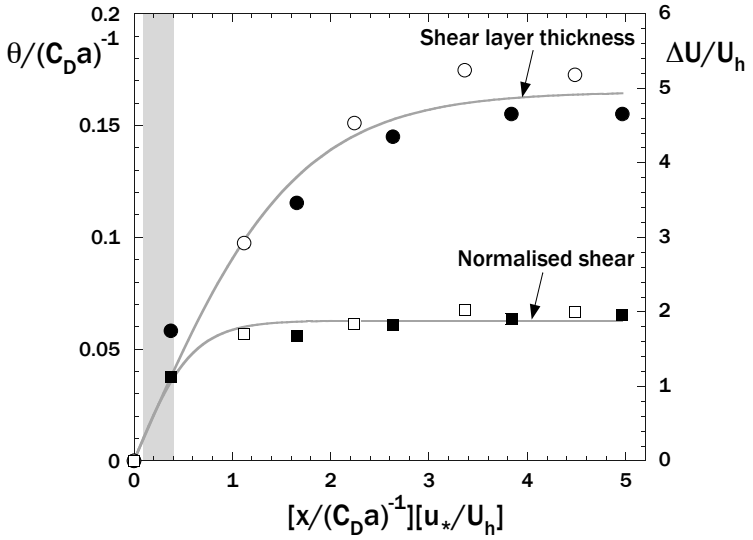

Fig. 8 The progression of shear layer momentum thickness (θ) and total shear (ΔU) along a waving canopy. The filled symbols represent Run FT1, the unfilled Run FT2. Distance from the front of the canopy (x) has been normalised according to the predicted scaling relationship for L_T (Equation (6)). The shaded region represents the deceleration length scale estimates for the two runs by Coceal and Belcher (2004). Deceleration of the in-canopy flow (and thus the increase of ΔU) occurs more rapidly than the spreading of the shear layer. Fully-developed canopy flow is reached at a distance $3(U_h/u_*)(C_D a)^{-1}$ from the front of the canopy.